


## Nonequilibrium thermal resistance of interfaces between III-V compounds

Jinchen Han<sup>1</sup> and Sangyeop Lee<sup>1,2,\*</sup><sup>1</sup>Department of Mechanical Engineering and Materials Science, University of Pittsburgh, Pittsburgh, Pennsylvania 15261, USA<sup>2</sup>Department of Physics and Astronomy, University of Pittsburgh, Pittsburgh, Pennsylvania 15261, USA (Received 20 September 2023; revised 13 November 2023; accepted 3 January 2024; published 26 January 2024)

In this paper, we report a systematic study on how vibrational spectra mismatch affects the degree of phonon nonequilibrium near an interface, how fast it is relaxed as the phonons diffuse into a lead, and the overall interfacial thermal resistance from the nonequilibrium phonons. Our discussion is based on the solution of the Peierls-Boltzmann transport equation with *ab initio* inputs for 36 interfaces between semi-infinite group-III (Al, Ga, In) and group-V (P, As, Sb) compound semiconductor leads. The simulation reveals that the nonequilibrium phonons cause significant interfacial thermal resistance for all 36 interfaces, making the overall interfacial thermal resistance two to three times larger than that predicted by the Landauer formalism. We observe a clear trend that the degree of phonon nonequilibrium near an interface and the interfacial thermal resistance from the nonequilibrium phonons increase as the mismatch of the Debye temperature of two lead materials increases. This contrasts with the Landauer formalism's predictions, which show no correlation with the Debye temperature mismatch. The relaxation length of the phonon nonequilibrium varies significantly from 50 nm to 1.5  $\mu\text{m}$  depending on the combination of the materials. The relaxation length is proportional to the phonon mean free path of the corresponding lead material but also largely depends on the material in the opposite lead. This suggests the relaxation length cannot be considered an intrinsic property of the corresponding lead material. These findings offer vital insights for understanding nonequilibrium effects on the interfacial thermal transport and optimizing thermal design in devices.

DOI: [10.1103/PhysRevMaterials.8.014604](https://doi.org/10.1103/PhysRevMaterials.8.014604)

## I. INTRODUCTION

The growing demand for highly integrated and miniaturized devices has catapulted interfacial thermal transport to the forefront of thermal management and energy conversion [1–4]. As device interface density increases, the efficiency and reliability of numerous technologies—such as microelectronics, photonics, and thermoelectrics—hinge on interfacial thermal transport [3–6]. However, understanding interfacial thermal transport is challenging, given complexities such as atomic structure mismatches and intricate heat carrier interactions at the interfaces [3–5]. Hence, a comprehensive theoretical understanding of interfacial thermal conductance is critical for optimizing thermal design [7].

Landauer formalism stands as a widely used and effective theoretical tool for assessing interfacial thermal resistance [8]. It assumes an equilibrium Bose-Einstein distribution ( $f^0$ ) with constant temperature in leads and a finite temperature drop at the interface to determine the interface thermal conductance [8]. However, two main limitations exist with this assumption: (i) the internal phonon scattering results in nonzero temperature gradients in both leads given nonzero heat flux, and (ii) the interface scattering induces nonequilibrium phonon distribution near the interface.

Regarding the first limitation, the Landauer formalism was modified such that ( $f^0$ ) is substituted with the bulk distribution  $f^{\text{bulk}}$  representing the phonon distribution in an infinitely

large sample under a homogeneous temperature gradient [9,10]. This  $f^{\text{bulk}}$  captures the phonons that are out of equilibrium due to the temperature gradient. However, considerable discrepancies exist between predictions from the modified Landauer formalism and outcomes from both nonequilibrium molecular dynamics (NEMD) simulations [11] and experimental data [12–14]. Furthermore, this modified Landauer formalism still neglects the nonequilibrium phonons caused by interface-phonon scattering.

The nonequilibrium phonons near interfaces have recently gained significant attention [15]. To clarify, when a temperature gradient exists, phonons in a bulk material without an interface exhibit an out-of-equilibrium distribution resulting from the balance between displacement by the temperature gradient and relaxation through scattering. Near an interface, the out-of-equilibrium state is excessively larger than that in the bulk material due to the reflection of phonons caused by phonon-interface scattering and the discontinuity of temperature across the interface. In this paper, the “nonequilibrium” refers to the excessive out-of-equilibrium state due to an interface. So far, various theoretical methods, including the multitemperature model (MTM) [16], NEMD simulation [17,18], and the Peierls-Boltzmann transport equation (PBE) [12,19–23], have been employed to investigate these phonon nonequilibrium effects. The MTM results showed that each branch of phonons exhibits different temperatures near the Si-Ge interface indicating local thermal nonequilibrium near the interface [16]. However, the MTM can underestimate the nonequilibrium effects because of its underlying assumption that all modes in the same branch or group are in equilibrium.

\*sylee@pitt.edu

The NEMD simulations can naturally involve all phonon anharmonicity and consider complex interfacial lattice structure. Previous studies utilizing modal or spectral analysis emphasize the significant effects of anharmonicity among phonon modes on thermal resistance [17,18]. However, for the NEMD to capture the out-of-equilibrium nature of phonons, the domain size should be larger than the mean free paths (MFPs) of phonons, which may require high computational cost. The typical domain size of the past NEMD studies involving Si is around 80 nm [11,17,24,25], not sufficiently large to capture heat-carrying phonons with long mean free paths which can be a few micrometers [26]. This often means the simulation results can depend on the system size. The PBE can describe much longer length scale and provide modal distribution function naturally. However, previous PBE studies do not include quantitative analysis of the thermal resistance from phonon nonequilibrium [20,23].

Recently, we solved the PBE with the kinetic Monte Carlo (MC) method and quantitatively showed the significant nonequilibrium thermal resistance at an interface shared by semi-infinite Si and Ge leads [12]. The study found that (i) the interface scattering leads to significant phonon nonequilibrium near the Si-Ge interface, (ii) as phonons diffuse from the interface, the nonequilibrium distribution is relaxed to the bulk distribution due to internal phonon scattering, and (iii) the entropy generation and consequent thermal resistance during this relaxation process can be substantial, given the large mismatch between the nonequilibrium distribution near the interface and  $f^{\text{bulk}}$  far away from the interface. Consequently, the relaxation of the nonequilibrium phonon distribution results in a higher thermal resistance than the interface scattering at the Si-Ge interface. Overall, when considering both mechanisms together—interface scattering and the relaxation of nonequilibrium phonons—the total interfacial thermal resistance of the Si-Ge interface is considerably larger than Landauer formalism's predictions. This observation naturally leads to the questions of whether the significant nonequilibrium resistance is common among many other interfaces. Also, the major factors that determine the degree of phonon nonequilibrium and its decay rate need to be identified.

In this study, we apply the established kinetic MC method to solve the steady-state PBE for 36 interfaces consisting of semi-infinite III-V leads. With the varying atomic mass

and interatomic force constants of III-V compounds, their 36 interfaces provide a systematic way of changing the phonon properties and studying their effects on the nonequilibrium phenomena for interfacial thermal transport. Moreover, the III-V compounds and their interfaces are of practical importance for electronic and photonic devices [27–29]. A deeper comprehension of their interfacial thermal transport can guide better device-level design for superior thermal management [29,30].

## II. METHOD

We solve the PBE for interfaces shared by semi-infinite III-V compound semiconductor leads at 300 K. We use the variance reduced kinetic MC method to solve the PBE as elaborated upon in prior studies [12,31]. The method only accounts for the deviational energy distribution from the global equilibrium (GEQ) distribution to reduce the variance. While the details of MC simulation for interfacial thermal transport can be found in our previous study [12], we will briefly discuss the method here. The deviational energy form of the steady-state PBE under the relaxation time approximation (RTA) can be written as

$$v_{x,i} \frac{de_i^d(x)}{dx} = -\frac{e_i^d(x) - e_i^{d,\text{loc}}(x)}{\tau_i}, \quad (1)$$

where  $v_{x,i}$  and  $\tau_i$  denote the phonon group velocity along the  $x$  direction and the lifetime of mode  $i$ , respectively.  $e_i^d(x)$  is the deviation of energy distribution from global equilibrium, which is  $\hbar\omega_i[f_i(x) - f_i^{\text{GEQ}}]$ . Here,  $\omega_i$  and  $f_i$  are the phonon frequency and distribution of mode  $i$ , and  $\hbar$  is the reduced Planck constant. The  $e_i^{d,\text{loc}}$  is the deviation of local equilibrium energy distribution ( $e_i^{\text{loc}}$ ) from the global equilibrium energy distribution ( $e_i^{\text{GEQ}}$ ), i.e.,  $e_i^{d,\text{loc}} = e_i^{\text{loc}}(x) - e_i^{\text{GEQ}}$ .

Our simulation assumes an interface at  $x = 0$ , shared by two semi-infinite leads. In practice, these semi-infinite leads are approximated as finite-length leads with lengths of  $L_1$  and  $L_2$ . Here, 1 and 2 denote the left-side and the right-side lead, respectively. These lengths uphold  $f^{\text{bulk}}$  with the assigned local temperatures  $T_H$  and  $T_C$  at the hot ( $x = -L_1$ ) and cold boundary ( $x = L_2$ ), respectively. As such, the sampling particles emitted from  $x = -L_1$  and  $x = L_2$  follow the boundary conditions:

$$e_i^d|_{x=-L_1} = \hbar\omega_i \left[ f_i^0(T_H) - v_{x,i}\tau_i \frac{\partial f_i^0}{\partial T} \frac{dT}{dx} - f_i^{\text{GEQ}} \right] \text{ for modes } i \text{ with } v_{x,i} > 0, \quad (2)$$

$$e_j^d|_{x=L_2} = \hbar\omega_j \left[ f_j^0(T_C) - v_{x,j}\tau_j \frac{\partial f_j^0}{\partial T} \frac{dT}{dx} - f_j^{\text{GEQ}} \right] \text{ for modes } j \text{ with } v_{x,j} < 0, \quad (3)$$

where  $f_i^0(T_H)$  and  $f_j^0(T_C)$  denote the Bose-Einstein distribution at  $T_H$  and  $T_C$  of two materials.  $i$  and  $j$  denote phonon modes of left lead 1 and right lead 2, respectively.

For the finite leads to represent the semi-infinite leads, the following two conditions should be satisfied. First, the length of the finite leads must ensure the nonequilibrium distribution near the interface is fully relaxed to  $f^{\text{bulk}}$  within

the finite lead. Each lead length for all cases is selected to be  $200\Lambda_{\text{avg}}$ , where  $\Lambda_{\text{avg}}$  is the mode-averaged MFP of phonons weighted by the modal specific heat, i.e.,  $\Lambda_{\text{avg}} = \sum_i \hbar\omega_i (\partial f_i^0 / \partial T) v_{x,i} \tau_i / \sum_i \hbar\omega_i (\partial f_i^0 / \partial T)$ . The  $\Lambda_{\text{avg}}$  and lead lengths for each III-V semiconductors are summarized in Supplemental Material Table I [32]. The second condition is about the temperature gradient at the boundary in Eqs. (2)

and (3). While the temperatures at the two boundaries,  $T_H$  and  $T_C$ , are assumed, the temperature gradients in Eqs. (2) and (3) are unknown and need to be found from the MC simulation. Thus, the PBE was solved iteratively with varying temperature gradient at the two boundaries until the actual temperature gradient matches with the one assumed for the boundary conditions.

All inputs for the PBE solver, including harmonic phonon properties and three-phonon scattering rates, are calculated from first principles via the VASP [33–36], PHONOPY [37], and SHENGBTE [38] packages. We employed the local density approximation (LDA) with the projector augmented wave method (PAW) as the exchange correlation functional [39,40]. The lattice structure is relaxed with a primitive cell until the energy change between two electronic steps is less than  $10^{-7}$  eV. The second- and third-order interatomic force constants (IFCs) are then obtained using finite-difference methods with a  $4 \times 4 \times 4$  supercell. The cutoff energy is 600 eV for both relaxation and the IFC calculation. The reciprocal space for electrons is sampled with a  $3 \times 3 \times 3$  mesh for the  $4 \times 4 \times 4$  supercell. For the third-order IFCs, we set the interaction cutoff range to include up to the third nearest neighbors following previous reports on the literature [41]. The calculated lattice constants and thermal conductivities are listed in Supplemental Material Table I [32]. The reciprocal space for phonons is sampled with a  $15 \times 15 \times 15$  mesh. The phonon transmission function across interfaces was calculated using the diffuse mismatch model (DMM) and *ab initio* phonon dispersion.

Thermophysical properties such as the local temperature  $T_{\text{loc}}$ , heat flux  $q''$ , local entropy generation rate  $\dot{S}$ , and thermal resistance  $R$  can be calculated by postprocessing the local phonon distribution from the MC solution of PBE. Each lead is divided into ten equal-sized control volumes that have a spatially averaged distribution function. The  $T_{\text{loc}}$  of each control volume was found as  $T_{\text{loc}} = (NV_{\text{uc}} \sum_i C_{V,i}/\tau_i)^{-1} \sum_i e_i^d/\tau_i$  [42,43], where  $N$  is the number of wave vectors in the reciprocal space,  $V_{\text{uc}}$  is the volume of the unit cell, and  $C_{V,i}$  is the volumetric specific heat of mode  $i$ .  $q''$  is calculated as  $q'' = (NV_{\text{uc}})^{-1} \sum_i v_{x,i} e_i^d$ . The total thermal resistance of the computational domain is  $R_{\text{tot}} = (T_H - T_C)/q''$ . This can be divided into two parts based on their mechanisms: (i) intrinsic thermal resistance  $R_{\text{bulk}}$  resulting from the bulk thermal resistivity, and (ii) the interfacial resistance  $R_{\text{int}}$  that is caused by the interface. The  $R_{\text{bulk}}$  is simply found as  $L_1^{-1} \kappa_1^{-1} + L_2^{-1} \kappa_2^{-1}$ , where  $\kappa$  is the thermal conductivity reflecting three-phonon scattering in bulk materials.  $R_{\text{int}}$  is obtained by subtracting  $R_{\text{bulk}}$  from  $R_{\text{tot}}$ . This resistance can be further divided into two parts with different mechanisms: (i) the resistance due to

the relaxation of highly nonequilibrium phonon distribution to bulk distribution by three-phonon scattering ( $R_{\text{neq}}$ ), and (ii) the resistance directly caused by the interface scattering ( $R_{\text{int}}^0$ ). The resistance of the whole domain including leads 1 and 2 now becomes  $R_{\text{tot}} = R_{\text{bulk},1} + R_{\text{neq},1} + R_{\text{int}}^0 + R_{\text{neq},2} + R_{\text{bulk},2}$ .

In practice,  $R_{\text{neq}}$  can be evaluated by calculating the local entropy generation rate due to the three-phonon scattering ( $\dot{S}$ ). The  $\dot{S}$  under RTA is [12,44]

$$\dot{S} = \frac{1}{NV_{\text{uc}} T_{\text{loc}}^2} \sum_i \frac{(e_i^d - e_i^{d,\text{loc}})^2}{(de_i^{\text{loc}}/dT)\tau_i}. \quad (4)$$

From the above expression, the entropy generation rate and thermal resistance can be large when the local energy distribution significantly deviates from the equilibrium distribution and the energy transfer rate to other modes through scattering is high. These two conditions are represented by  $(e_i^d - e_i^{d,\text{loc}})$  and  $(e_i^d - e_i^{d,\text{loc}})/\tau_i$  in Eq. (4), respectively.

The rate of entropy generation in bulk material without interface ( $\dot{S}_{\text{bulk}}$ ) can be found using  $e_i^d = e_i^{\text{bulk}} - e_i^{\text{GEQ}}$  in Eq. (4). Thus,  $\dot{S} - \dot{S}_{\text{bulk}}$  is the additional entropy generation rate due to the relaxation of nonequilibrium phonons to bulk distribution. The local resistivity from the relaxation process of nonequilibrium phonons ( $R'_{\text{neq}}$ ) can be then calculated as  $(T_{\text{loc}}/q'')^2 (\dot{S} - \dot{S}_{\text{bulk}})$ . The thermal resistance from nonequilibrium phonons  $R_{\text{neq},X}$  of material  $X$  is simply obtained by spatially integrating  $R'_{\text{neq},X}$ . Finally, the  $R_{\text{int}}^0$  can be found by subtracting  $R_{\text{bulk}}$  and  $R_{\text{neq},A+B}$  (the sum of  $R_{\text{neq}}$  of material  $A$  and  $B$ ) from  $R_{\text{tot}}$ .

We considered eight zinc-blende III-V compounds, which are AlP, GaP, InP, AlAs, GaAs, InAs, GaSb, and InSb. We excluded AlSb since the RTA is known to fail for this material [41]. These eight materials can form 28 heterostructure interfaces and eight homojunction interfaces.

### III. RESULTS AND DISCUSSION

Figure 1(a) illustrates a comparison between the interfacial thermal resistance obtained from the MC simulation and the Landauer formalism combined with DMM, denoted as  $R_{\text{int}}$  and  $R_L$ , respectively. Notably,  $R_{\text{int}}$  values are larger than those of  $R_L$  by approximately threefold across all 36 interfaces. Figures 1(b) and 1(c) break down  $R_{\text{int}}$  into  $R_{\text{int}}^0$  and  $R_{\text{neq},A+B}$ , revealing that the considerable nonequilibrium effects contribute to the difference between  $R_{\text{int}}$  and  $R_L$ .

In Fig. 1(b),  $R_{\text{int}}^0$  differs substantially from  $R_L$ , particularly for interfaces of X-InAs and X-InSb (pink and red points). The  $R_L$  can be expressed as

$$R_L = \lim_{\Delta T \rightarrow 0} \Delta T \left( \frac{1}{N_1 V_{\text{uc},1}} \sum_{i, v_{x,i} > 0} v_{x,i} e_i^{d,\text{loc}} \Big|_{x=0-t_{i,1 \rightarrow 2}} - \frac{1}{N_2 V_{\text{uc},2}} \sum_{j, v_{x,j} < 0} v_{x,j} e_j^{d,\text{loc}} \Big|_{x=0+t_{j,2 \rightarrow 1}} \right)^{-1}, \quad (5)$$

where  $\Delta T$  is the temperature difference across the interface;  $t_{i,1 \rightarrow 2}$  and  $t_{j,2 \rightarrow 1}$  are the transmission function of mode  $i$  from lead 1 to 2 and mode  $j$  from lead 2 to 1, respectively. Using the fact that the net heat flux is zero when two leads are at the same temperature, Eq. (5) is usually simplified to  $R_L = N_1 V_{\text{uc},1} [\sum_{i, v_{x,i} > 0} v_{x,i} (de_i^0/dT) t_{i,1 \rightarrow 2}]^{-1}$  [45]. Similar to Eq. (5),  $R_{\text{int}}^0$  in the MC

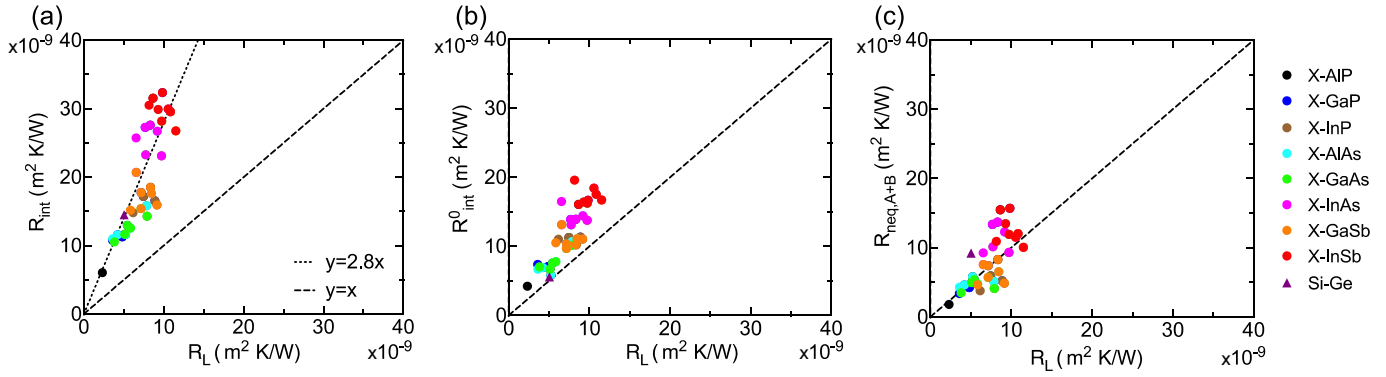


FIG. 1. The thermal resistances from the PBE compared to those from the Landauer formalism: (a) overall interfacial thermal resistance ( $R_{\text{int}}$ ), (b) resistance directly caused by interface scattering ( $R_{\text{int}}^0$ ), and (c) nonequilibrium thermal resistance in two leads ( $R_{\text{neq},A+B}$ ). The  $R_L$  is the resistance from the Landauer formalism. In the legend, the  $X$  signifies any III-V compound. Note that heterogeneous interfaces are shown twice; for example, the AIP-AlAs interface is shown as  $X$ -AIP and  $X$ -AlAs. For comparison, the Si-Ge interface is represented by a purple triangle [12].

simulation can be expressed as

$$R_{\text{int}}^0 = \lim_{\Delta T \rightarrow 0} \Delta T \left( \frac{1}{N_1 V_{\text{uc},1}} \sum_{i, v_{x,i} > 0} v_{x,i} e_i^d \Big|_{x=0^-} t_{i,1 \rightarrow 2} - \frac{1}{N_2 V_{\text{uc},2}} \sum_{j, v_{x,j} < 0} v_{x,j} e_j^d \Big|_{x=0^+} t_{j,2 \rightarrow 1} \right)^{-1}. \quad (6)$$

Equation (6) can be further simplified using  $e_i^d = e_i^{d,\text{loc}} + \Delta e_i^d$  and  $e_j^d = e_j^{d,\text{loc}} + \Delta e_j^d$  as

$$R_{\text{int}}^0 = \left[ R_L^{-1} + \lim_{\Delta T \rightarrow 0} \Delta T \left( \frac{1}{N_1 V_{\text{uc},1}} \sum_{i, v_{x,i} > 0} v_{x,i} \Delta e_i^d \Big|_{x=0^-} t_{i,1 \rightarrow 2} - \frac{1}{N_2 V_{\text{uc},2}} \sum_{j, v_{x,j} < 0} v_{x,j} \Delta e_j^d \Big|_{x=0^+} t_{j,2 \rightarrow 1} \right)^{-1} \right]^{-1}, \quad (7)$$

where  $\Delta e_i^d$  and  $\Delta e_j^d$  are the nonequilibrium portions of the distribution functions. Equation (7) shows that  $R_{\text{int}}^0$  depends not only the equilibrium distribution change resulting from temperature drop across the interface ( $R_L^{-1}$ ) but also on the nonequilibrium distribution  $\Delta e_i^d$  and  $\Delta e_j^d$  at  $x = 0$ .

The Landauer formalism ignores the latter in Eq. (7) as it assumes the equilibrium distributions in two leads. Our previous results of Si-Ge interface indicate a negligible difference between  $R_{\text{int}}^0$  and  $R_L$ , as plotted with a triangle in Fig. 1(b) [12]. This suggests that, for the Si-Ge interface, the equilibrium component primarily drives the change in phonon distribution across the interface. However, when considering 36 interfaces of various III-V compounds in this work, most of the interfaces exhibit significant differences between  $R_{\text{int}}^0$  and  $R_L$ . This indicates that changes in the nonequilibrium component across the interface can be as significant as the equilibrium component change. Thus,  $R_{\text{int}}^0$  depends on both the transmission function and the on-site phonon nonequilibrium distribution.

Another reason for  $R_{\text{int}}$  being larger than  $R_L$  is  $R_{\text{neq},A+B}$ . As shown in Fig. 1(c), the  $R_{\text{neq},A+B}$  is comparable to  $R_L$  for all interfaces we studied, similar to the previously studied Si-Ge case [12]. The data from the 36 interfaces in Fig. 1(c) underscore the importance of the nonequilibrium effect in predicting and understanding the interfacial thermal resistance in general.  $R_{\text{neq},A+B}$  and  $R_L$  have a positive correlation, indicating

that the interfaces with a larger  $R_L$  exhibit a more pronounced nonequilibrium effect.

We confirm that the nonequilibrium effects play a significant role in interfacial thermal resistance. However, calculating  $R_{\text{neq},A+B}$  can be complex since it necessitates solving the PBE in both real and reciprocal spaces. Thus, a simple indicator for  $R_{\text{neq},A+B}$ , if one exists, would be helpful to roughly estimate the nonequilibrium effect. The Debye temperature ratio of the constituent materials can be considered as a viable indicator because it approximately captures the mismatch of acoustic vibrational spectra between two materials. The Debye temperature can serve as a rough measure of acoustic phonon properties to estimate thermal conductivity [46] and the interfacial thermal conductance within the elastic interfacial scattering scheme [3]. In this study, we calculate the Debye temperature using elastic constants from first principles [47,48], and the Debye temperature values for all studied materials are available in Supplemental Material Table I [32]. We then define the Debye temperature ratio  $\Theta_A/\Theta_B$  as the higher Debye temperature divided by the lower one for a given interface. This ensures that  $\Theta_A/\Theta_B$  is always greater than or equal to 1. The subscripts  $A$  and  $B$  denote the constituent materials with higher and lower Debye temperatures, respectively.

Figure 2 shows  $\Theta_A/\Theta_B$  to be an effective indicator for estimating  $R_{\text{neq},A+B}$ , while it is not for  $R_L$  and  $R_{\text{int}}^0$ . It appears in Figs. 2(a) and 2(b) that neither  $R_L$  nor  $R_{\text{int}}^0$  has a clear

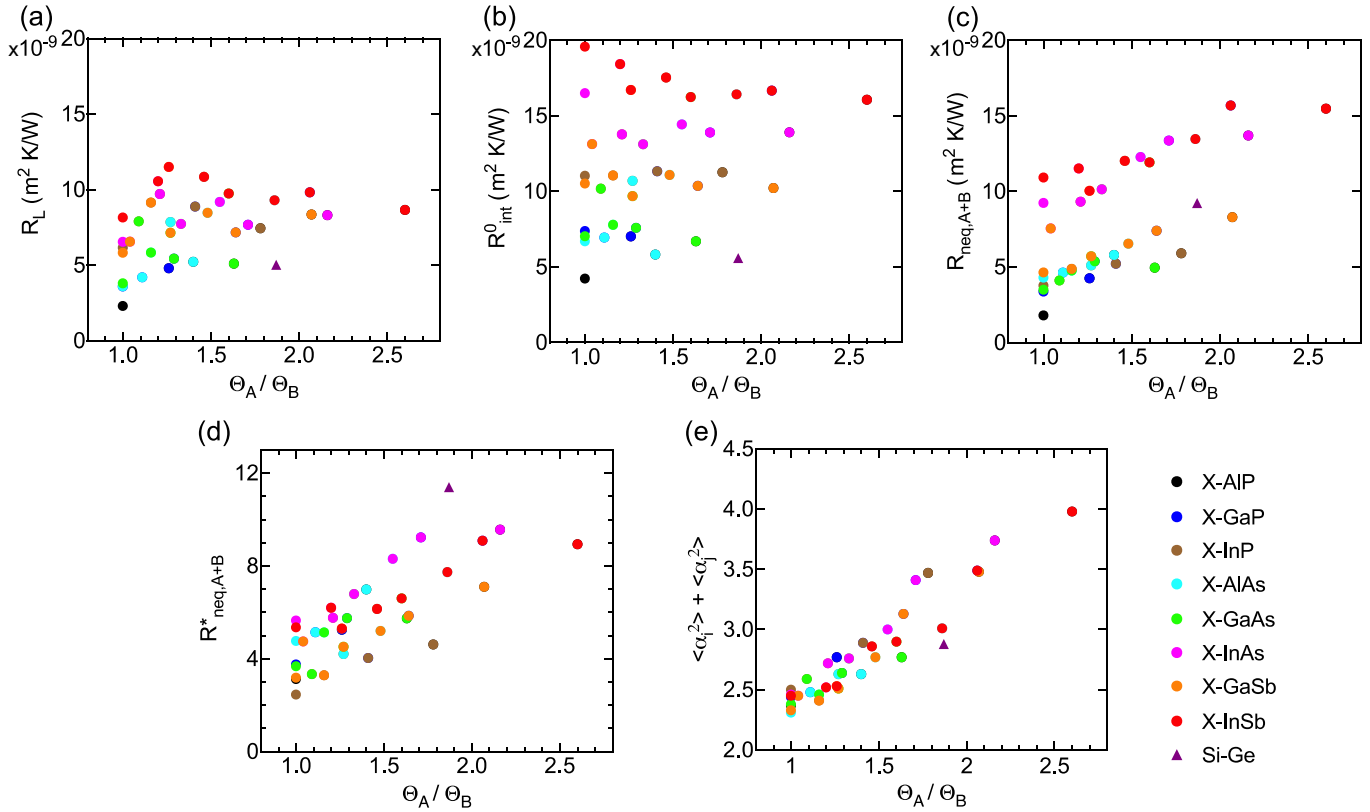


FIG. 2. The resistance versus the Debye temperature ratio  $\Theta_A/\Theta_B$  between two lead materials: (a) resistance predicted by Landauer formalism with DMM model  $R_L$ , (b) resistance directly induced by interface scattering  $R_{\text{int}}^0$ , (c) nonequilibrium resistance  $R_{\text{neq},A+B}$ , (d) dimensionless nonequilibrium resistance  $R_{\text{neq},A+B}^*$  representing  $\langle (\alpha_i^2 - 1)\beta_i \rangle + \langle (\alpha_j^2 - 1)\beta_j \rangle$ , and (e) the degree of nonequilibrium distribution at the interface  $\langle \alpha_i^2 \rangle + \langle \alpha_j^2 \rangle$ .

correlation with  $\Theta_A/\Theta_B$ . This absence of correlation arises since optical modes carry significant heat in the Landauer formalism with DMM. For instance, the optical modes of InSb contribute 13%–44% to the total heat flux in X-InSb interfaces. Therefore, the Debye temperature ratio, emphasizing only the acoustic mode mismatch, does not clearly correlate with resistance values derived from Landauer formalism. However, Fig. 2(c) shows a clear correlation between  $\Theta_A/\Theta_B$  and  $R_{\text{neq},A+B}$ , indicating that the mismatch of acoustic vibrational spectra is closely related to the nonequilibrium resistance. In contrast to the Landauer formalism's case, the optical phonons carry minimal heat, attributed to the short mean free paths of the optical phonons when considering the internal phonon scattering. For instance, the optical modes of InSb contribute less than 5% to the heat flux in X-InSb interfaces as will be shown later in Fig. 5(d).

In Fig. 2(c), the  $R_{\text{neq},A+B}$  of all 36 interfaces are clustered into two distinct groups (red/pink and other colors). We propose a dimensionless resistance,  $R_{\text{neq},A+B}^*$ , defined as  $R_{\text{neq},A}/R_{b,A} + R_{\text{neq},B}/R_{b,B}$ . Here,  $R_{b,X}$  represents the ballistic resistance of material X, expressed as  $R_{b,X} = NV_{\text{uc}}[\sum_i |v_{x,i}|(de_i^0/dT)]^{-1}$ , to eliminate the effects of different group velocity and specific heat of lead materials. Figure 2(d) compares the  $R_{\text{neq},A+B}^*$  with the Debye temperature ratio. In contrast to  $R_{\text{neq},A+B}$ , the dimensionless nonequilibrium resistance does not exhibit two distinct groupings; instead, all 36 interfaces cluster into one group, demonstrat-

ing a clear positive correlation with the Debye temperature ratio.

The dimensionless nonequilibrium resistance contains two important parameters that decide the  $R_{\text{neq},X}$ : the degree of nonequilibrium distribution at the interface and its duration in space as phonons diffuse into a lead. Using the right lead as an example, the local nonequilibrium resistivity at the interface can be written as

$$R'_{\text{neq}}|_{x=0^+} = \left(\frac{T_{\text{loc}}}{q''}\right)^2 \frac{k_B}{NV_{\text{uc}}} \times \sum_i \frac{(f_i - f_i^0)^2 - (f_i^{\text{bulk}} - f_i^0)^2}{f_i^0(f_i^0 + 1)\tau_i} \Big|_{x=0^+}. \quad (8)$$

By introducing a function  $\alpha_i$ , defined as  $(f_i - f_i^0)^2|_{x=0^+} = \alpha_i^2(f_i^{\text{bulk}} - f_i^0)^2|_{x=0^+}$ , we can simplify Eq. (8) to

$$R'_{\text{neq}}|_{x=0^+} = \left(\frac{T_{\text{loc}}}{q''}\right)^2 \frac{k_B}{NV_{\text{uc}}} \sum_i \frac{(\alpha_i^2 - 1)(f_i^{\text{bulk}} - f_i^0)^2}{f_i^0(f_i^0 + 1)\tau_i} \Big|_{x=0^+}. \quad (9)$$

$\alpha_i$  represents the degree of nonequilibrium distribution at the interface  $x = 0^+$ . We then assume exponential decay of the nonequilibrium resistivity in space with a decay parameter  $\beta_i$ . The local nonequilibrium resistivity at any position  $x$  can

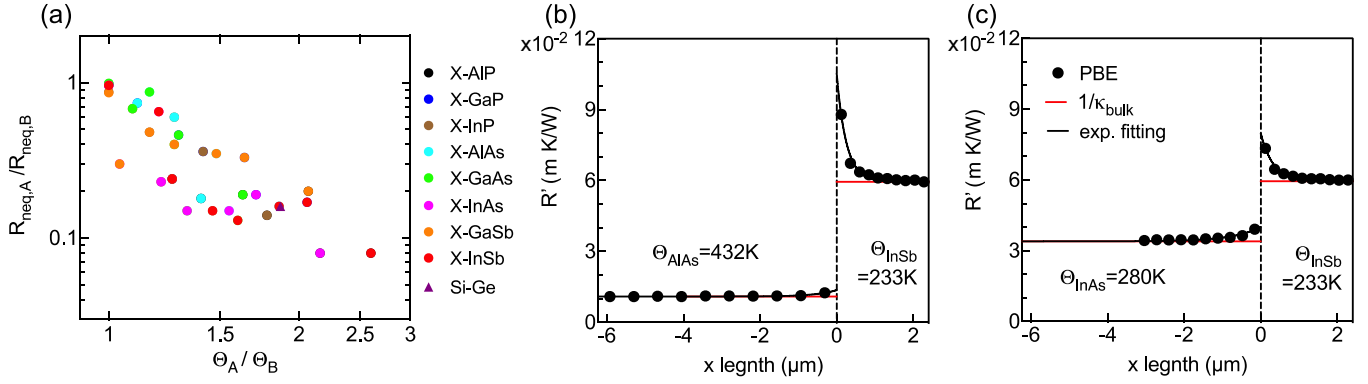


FIG. 3. (a) The nonequilibrium resistance ratio  $R_{\text{neq},A}/R_{\text{neq},B}$  versus the Debye temperature ratio  $\Theta_A/\Theta_B$ . The thermal resistivity  $R'$  for (b) the AlAs-InSb interface and (c) the InAs-InSb interface. In (b,c), the black solid circles represent PBE data, black lines indicate their exponential fits, and the red line denotes the thermal resistivity of bulk materials.

be written as

$$R'_{\text{neq}}|_x = \left(\frac{T_{\text{loc}}}{q''}\right)^2 \frac{k_B}{NV_{\text{uc}}} \sum_i \frac{(\alpha_i^2 - 1)(f_i^{\text{bulk}} - f_i^0)^2}{f_i^0(f_i^0 + 1)\tau_i} \Big|_{x=0^+} \times \exp\left(-\frac{x}{\beta_i|v_{x,i}|\tau_i}\right). \quad (10)$$

The parameter  $\beta_i$  signifies the decay rate of a specific modal nonequilibrium resistivity  $R'_{\text{neq},i}|_{x=0^+}$  in space relative to its mean free path  $|v_{x,i}|\tau_i$ . The assumption of exponential decay is well justified by the MC simulation results of Si-Ge interfaces in our previous work [12] and current work for III-V interfaces shown in Figs. 3(b) and 3(c). The nonequilibrium resistance of the right lead is written as

$$R_{\text{neq}} = \int_0^\infty R'_{\text{neq}}|_x dx = \sum_i R'_{\text{neq},i}|_{x=0^+} \beta_i |v_{x,i}|\tau_i. \quad (11)$$

We replace the heat flux  $q''|_{x=0^+}$  with the heat flux of bulk distribution  $q''|_{x \rightarrow \infty} = (NV_{\text{uc}})^{-1} \sum_i \hbar\omega_i v_{x,i}^2 \tau_i (df_i^0/dT) (-dT/dx)$ . Then, after normalizing  $R_{\text{neq}}$  with  $R_b$  as aforementioned, the dimensionless nonequilibrium resistance  $R_{\text{neq}}^*$  can be written as

$$R_{\text{neq}}^* = \frac{\sum_i (\alpha_i^2 - 1) \beta_i \hbar\omega_i v_{x,i}^2 |v_{x,i}|\tau_i^2 (df_i^0/dT)}{[\sum_i \hbar\omega_i v_{x,i}^2 \tau_i (df_i^0/dT)]^2 [\sum_i \hbar\omega_i |v_{x,i}| (df_i^0/dT)]^{-1}}. \quad (12)$$

Thus, the dimensionless nonequilibrium resistance is the mode average of  $(\alpha_i^2 - 1)\beta_i$ . Thus,  $R_{\text{neq},A+B}^*$  can be written as  $\langle(\alpha_i^2 - 1)\beta_i\rangle + \langle(\alpha_j^2 - 1)\beta_j\rangle$  where the angle bracket denotes mode average. Figure 2(d) clearly shows that the combined average of  $\alpha$  and  $\beta$ , represented by  $R_{\text{neq},A+B}^*$  increases as the two leads have more significant mismatch of the acoustic vibrational spectra.

We further focus on the degree of nonequilibrium at the interface,  $\langle\alpha^2\rangle$ , which can be estimated by normalizing the nonequilibrium resistivity at the interface by the bulk resistivity of the lead. Using Eq. (9) and  $R'_{\text{bulk}} = NV_{\text{uc}}[\sum_i \hbar\omega_i v_{x,i}^2 \tau_i (df_i^0/dT)]^{-1}$ , the dimensionless resistivity

at  $x = 0^+$  is written as

$$\frac{R'_{\text{neq}}|_{x=0^+}}{R'_{\text{bulk}}} = \frac{\sum_i (\alpha_i^2 - 1) \hbar\omega_i v_{x,i}^2 \tau_i (df_i^0/dT)}{\sum_i \hbar\omega_i v_{x,i}^2 \tau_i (df_i^0/dT)}, \quad (13)$$

which represents the mode average of  $\alpha_i^2 - 1$ . Thus,  $\alpha_i^2 - 1$  can be calculated as  $R'_{\text{neq}}|_{x=0^+}/R'_{\text{bulk}} + 1$ . In this work,  $R'_{\text{neq}}|_{x=0^+}$  or  $R'_{\text{neq}}|_{x=0^-}$  is calculated by fitting  $R'_{\text{neq}}$  of control volumes with an exponential function.

Figure 2(e) plots the degree of nonequilibrium distribution at the interface  $\langle\alpha_i^2\rangle + \langle\alpha_j^2\rangle$  versus the Debye temperature ratio. We observe a strong positive correlation between  $\langle\alpha_i^2\rangle + \langle\alpha_j^2\rangle$  and  $\Theta_A/\Theta_B$ , suggesting that the acoustic vibrational mismatch is a deterministic factor for the phonon nonequilibrium at an interface. Figure 2(e) also reveals that the phonon distribution at the interface is highly nonequilibrium in all interfaces. The values of  $\langle\alpha_i^2\rangle + \langle\alpha_j^2\rangle$  range from 2.5 to 4, meaning that the deviation of phonon distribution from equilibrium at the interface is up to twice as large as the deviation in bulk case.

Comparing  $R_{\text{neq},A}$  and  $R_{\text{neq},B}$  across interfaces, we observe that  $R_{\text{neq}}$  is always more pronounced in the constituent material  $B$  with the lower Debye temperature. In Fig. 3(a), the ratios of the nonequilibrium resistances,  $R_{\text{neq},A}/R_{\text{neq},B}$ , are plotted against  $\Theta_A/\Theta_B$ .  $R_{\text{neq},A}/R_{\text{neq},B}$  is less than 1 for all interfaces, indicating that material  $A$  with the higher Debye temperature has a lower nonequilibrium resistance. Moreover,  $R_{\text{neq},A}/R_{\text{neq},B}$  has a negative correlation with  $\Theta_A/\Theta_B$ . The relationship can be understood by the two different ways the group velocity affects the nonequilibrium resistance. First, the lead with a lower group velocity exhibits a larger degree of nonequilibrium near the interface. This is because of the energy conservation, which dictates the same spectral heat flux across the interface with the assumption of elastic interface scattering, i.e.,  $\sum_i v_{x,i} e_i^d \delta(\omega_i - \omega) = \sum_j v_{x,j} e_j^d \delta(\omega_j - \omega)$  for any frequency  $\omega$  [12]. Material  $B$  with a lower  $v_x$  requires a larger deviational distribution  $e^d$  at the interface to maintain the same spectral heat flux, thereby generating more substantial entropy based on Eq. (6). On the other hand, the lower  $v_x$  shortens the relaxation length of the nonequilibrium distribution, which can reduce the overall  $R_{\text{neq}}$ . However, the degree of nonequilibrium near the interface is a bigger contributor to the overall  $R_{\text{neq}}$  compared to the relaxation length.

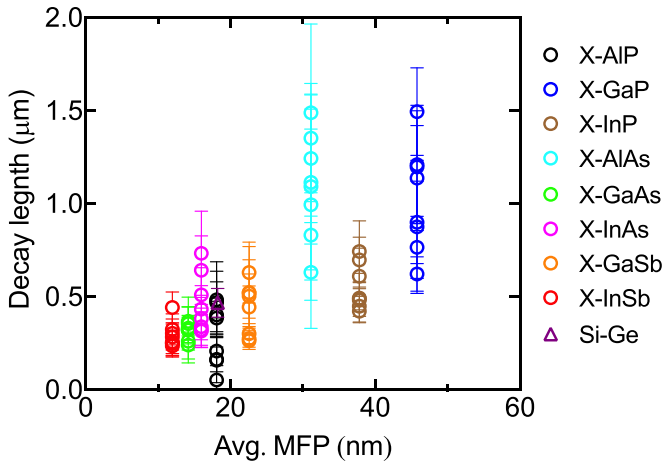


FIG. 4. The relaxation lengths of nonequilibrium resistivity in the right lead compared to the mode-averaged mean free paths of the corresponding lead materials.

We briefly show this using a gray model in the Sec. 2 of Supplemental Material. Figures 3(b) and 3(c) showcase the resistivity  $R'$  (black dots) and its exponential fit (black line) across the AlAs-InSb and InAs-InSb interfaces. The area between the black and red horizontal lines represents  $R_{\text{neq}}$ . In

both heterostructures,  $R_{\text{neq,InSb}}$  is significantly larger than both  $R_{\text{neq,AlAs}}$  and  $R_{\text{neq,InAs}}$  since the degree of nonequilibrium near the interface, represented by  $R'_{\text{neq}}$  at  $x=0$ , is significantly larger in InSb than in AlAs and InAs.

We now turn our attention to the decay length of the nonequilibrium resistivity.  $R'_{\text{neq}}$  can be fitted well with an exponential function,  $R'_{\text{neq},i}|_{x=0^+} \exp(-x/\lambda)$ , as depicted in Figs. 3(b) and 3(c). Here we define the fitting coefficient  $\lambda$  as a relaxation length. Figure 4 plots  $\lambda$  versus  $\Lambda_{\text{avg}}$  of the lead. The error bar shows the 95% confidence bounds of the fitting coefficient  $\lambda$ . Generally,  $\lambda$  is proportional to the  $\Lambda_{\text{avg}}$  of the corresponding lead material. It is worth noting that  $\lambda$  also depends on the material in the opposite lead. For example,  $\lambda$  in AIP of X-AIP varies by a factor of 10 depending on the material X in the opposite lead. For all interfacial structures,  $\lambda$  varies by a factor of at least 2–3. Therefore, the relaxation length  $\lambda$  in a lead is not an intrinsic property of the corresponding lead material, but rather depends on the combination of the two materials that constitute the interface.

Like the degree of nonequilibrium distribution represented by  $\langle \alpha_i^2 \rangle$ , the relaxation length  $\lambda$  is also influenced by the Debye temperature ratio. Figure 5 details the relaxation lengths of InSb ( $\lambda_{\text{InSb}}$ ) for all X-InSb interfaces. We chose InSb as the lead of interest since it has the lowest Debye temperature among the III-V compounds we studied and thus is expected

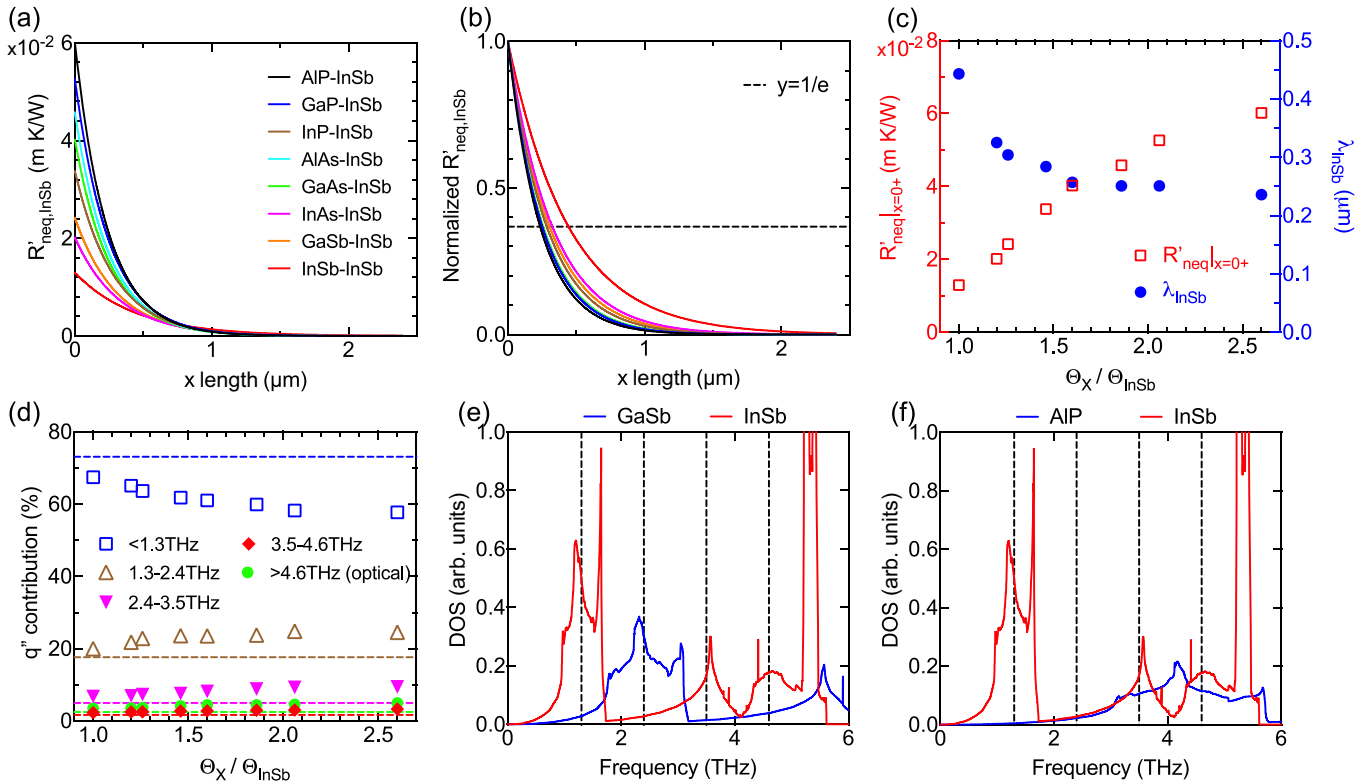


FIG. 5. Effects of lead material X on the nonequilibrium resistivity and its decay in X-InSb interfaces. [(a), (b)] Spatial decay of nonequilibrium resistivity in the InSb lead. The horizontal dashed line in (b) represents  $y = 1/e$  to indicate the relaxation length. (c) The nonequilibrium resistivity at the interface (red open squares) and relaxation length (blue solid circles) in InSb with respect to the Debye temperature ratio for different X-InSb interfaces. (d) Heat flux contribution from five frequency bins sampled at the control volume of InSb closest to the interface. The dashed lines represent the spectral heat flux contribution at the boundary of the InSb lead which is far from the interface and exhibits the bulk phonon distribution. [(e), (f)] Overlap of phonon density of states in GaSb-InSb ( $\Theta_{\text{GaSb}}/\Theta_{\text{InSb}} = 1.26$ ) and AIP-InSb ( $\Theta_{\text{AIP}}/\Theta_{\text{InSb}} = 2.6$ ) interfaces. The vertical dashed lines are the boundaries of the five frequency bins used in (d).

to exhibit the largest nonequilibrium effects as observed in Fig. 3. Figure 5(a) shows the exponential fitting of the nonequilibrium resistivity  $R'_{\text{neq,InSb}}$  in all  $X$ -InSb interfaces. The nonequilibrium resistivity at the interface,  $R'_{\text{neq}}|_{x=0^+}$ , has the largest value in the AIP-InSb heterostructure, gradually decreases as the Debye temperature difference between  $X$  and InSb decreases, and has the lowest value in the InSb-InSb interface. In Fig. 5(b), we normalize  $R'_{\text{neq,InSb}}$  by  $R'_{\text{neq}}|_{x=0^+}$  to compare  $\lambda_{\text{InSb}}$ .  $\lambda_{\text{InSb}}$  has the opposite trend as  $R'_{\text{neq}}|_{x=0^+}$ ; it is largest in the InSb-InSb and smallest in the AIP-InSb. Figure 5(c) summarizes both  $R'_{\text{neq}}|_{x=0^+}$  and  $\lambda_{\text{InSb}}$  shown in Figs. 5(a) and 5(b) as functions of  $\Theta_X/\Theta_{\text{InSb}}$ .  $R'_{\text{neq}}|_{x=0^+}$  increases with  $\Theta_X/\Theta_{\text{InSb}}$ , indicating that a larger acoustic mismatch results in a more out-of-equilibrium phonon distribution at the interface.  $\lambda_{\text{InSb}}$  decreases with  $\Theta_X/\Theta_{\text{InSb}}$  in  $X$ -InSb interface structures.

The dependence of relaxation length on the Debye temperature can be understood by measuring the spectral contribution to the thermal transport. The phonon mean free path varies significantly with the phonon frequency in a material. Consequently, the relaxation length of phonon nonequilibrium can vary based on the spectral heat flux distribution near the interface. Figure 5(d) showcases the spectral heat flux in the control volume centered at  $x = 0.12 \mu\text{m}$  which is adjacent to the interface ( $x = 0-0.24 \mu\text{m}$ ) in the InSb lead. We divide the entire phonon spectrum of InSb into five frequency bins and plot the contribution from each bin to the heat flux. The spectral heat flux in Fig. 5(d) is similar to the bulk case when  $\Theta_X/\Theta_{\text{InSb}}$  is close to 1. However, with an increase in  $\Theta_X/\Theta_{\text{InSb}}$ , contributions from low frequencies diminish, while those from high frequencies grow. This is because the Debye temperature ratio greatly influences the spectral overlap of phonon density of states (DOS). In turn, this overlap dictates the spectral transmission function in DMM.

Comparison of GaSb-InSb and AIP-InSb in Figs. 5(e) and 5(f) further clarifies the vibrational spectra mismatch and its effects on the spectral heat flux distribution and the relaxation length of phonon nonequilibrium. The GaSb-InSb interface has a considerable overlap of phonon DOS in the low frequency range while the overlap in the AIP-InSb interface mostly occurs in a much higher frequency range. This leads to the different spectral heat flux distributions in GaSb-InSb and AIP-InSb in Fig. 5(d); the low frequency phonons with long mean free paths carry more heat in GaSb-InSb than in AIP-InSb. As a result, the relaxation length is larger in GaSb-InSb than in AIP-InSb, as shown in Fig. 5(c).

#### IV. CONCLUSION

In this work, we comprehensively analyzed the thermal resistance across 36 III-V interfaces by solving the Peierls-Boltzmann transport equation with *ab initio* phonon dispersion and three-phonon scattering rates. The DMM is assumed for the phonon transmission across the interface. Our simulations revealed significant nonequilibrium effects for the interfacial thermal resistance. For all 36 interfaces, the overall interfacial thermal resistance considering nonequilibrium phonons is two to three times larger than the interfacial thermal resistance by the Landauer formalism which assumes equilibrium distribution of phonons. We also found the nonequilibrium effect is always pronounced in a lead with lower Debye temperature between two leads constituting the interface. Using the dimensionless form of nonequilibrium resistance, we estimated the degree of phonon nonequilibrium near the interface. All 36 interfaces show a clear correlation between the degree of phonon nonequilibrium near the interface and the Debye temperature mismatch; this indicates that the acoustic vibrational spectra mismatch is the main factor that determines the nonequilibrium phonons and hence interfacial thermal resistance. This contrasts with the Landauer formalism from which interfacial resistance shows no correlation with the Debye temperature mismatch. The relaxation lengths of the nonequilibrium phonons are discussed to identify the extent of space where the nonequilibrium effect is significant. Depending on the interface, the relaxation length varies between 50 nm and 1.5  $\mu\text{m}$ . In general, while the relaxation length is proportional to the phonon mean free paths of the corresponding lead material, it also heavily depends on the material in the opposite lead. A mismatch of acoustic vibrational spectra alters the spectral distribution of the heat flux. Given the strong function of the phonon mean free path with respect to the phonon frequency, this results in the largely varying relaxation length of nonequilibrium phonons depending on the combination of lead materials.

#### ACKNOWLEDGMENTS

We thank Richard Wilson and Yee Kan Koh for helpful discussions. We acknowledge support from the National Science Foundation (Award No. 1943807). This research was also supported in part by the University of Pittsburgh Center for Research Computing, Award No. RRID:SCR\_022735, through the resources provided. Specifically, this work used the H2P cluster, which is supported by National Science Foundation Award No. OAC-5512117681.

- 
- [1] D. G. Cahill, P. V. Braun, G. Chen, D. R. Clarke, S. Fan, K. E. Goodson, P. Keblinski, W. P. King, G. D. Mahan, A. Majumdar *et al.*, *Appl. Phys. Rev.* **1**, 011305 (2014).
  - [2] D. G. Cahill, W. K. Ford, K. E. Goodson, G. D. Mahan, A. Majumdar, H. J. Maris, R. Merlin, and S. R. Phillpot, *J. Appl. Phys.* **93**, 793 (2003).
  - [3] A. Giri and P. E. Hopkins, *Adv. Funct. Mater.* **30**, 1903857 (2020).
  - [4] C. Monachon, L. Weber, and C. Dames, *Annu. Rev. Mater. Res.* **46**, 433 (2016).
  - [5] J. Chen, X. Xu, J. Zhou, and B. Li, *Rev. Mod. Phys.* **94**, 025002 (2022).
  - [6] R. J. Warzoha, A. A. Wilson, B. F. Donovan, N. Donmez, A. Giri, P. E. Hopkins, S. Choi, D. Pahinkar, J. Shi, S. Graham *et al.*, *J. Electron. Packag.* **143**, 020804 (2021).



- [7] P. Zhang, P. Yuan, X. Jiang, S. Zhai, J. Zeng, Y. Xian, H. Qin, and D. Yang, *Small* **14**, 1702769 (2018).
- [8] Y. Imry and R. Landauer, *Rev. Mod. Phys.* **71**, S306 (1999).
- [9] S. Simons, *J. Phys. C: Solid State Phys.* **7**, 4048 (1974).
- [10] G. Chen, *Appl. Phys. Lett.* **82**, 991 (2003).
- [11] E. S. Landry and A. J. H. McGaughey, *Phys. Rev. B* **80**, 165304 (2009).
- [12] X. Li, J. Han, and S. Lee, *Mater. Today Phys.* **34**, 101063 (2023).
- [13] Z. Cheng, R. Li, X. Yan, G. Jernigan, J. Shi, M. E. Liao, N. J. Hines, C. A. Gadre, J. C. Idrobo, E. Lee *et al.*, *Nat. Commun.* **12**, 6901 (2021).
- [14] S. M. Lee, D. G. Cahill, and R. Venkatasubramanian, *Appl. Phys. Lett.* **70**, 2957 (1997).
- [15] Z. Lu and X. Ruan, *ES Energy Environ.* **4**, 5 (2019).
- [16] Z. Lu, J. Shi, and X. Ruan, *J. Appl. Phys.* **125**, 085107 (2019).
- [17] T. Feng, Y. Zhong, J. Shi, and X. Ruan, *Phys. Rev. B* **99**, 045301 (2019).
- [18] T. Feng, W. Yao, Z. Wang, J. Shi, C. Li, B. Cao, and X. Ruan, *Phys. Rev. B* **95**, 195202 (2017).
- [19] W. Bao, Z. Wang, and D. Tang, *Int. J. Heat Mass Transfer* **183**, 122090 (2022).
- [20] J. Xu, Y. Hu, X. Ruan, X. Wang, T. Feng, and H. Bao, *Phys. Rev. B* **104**, 104310 (2021).
- [21] S. Lee, X. Li, and R. Guo, *Nanoscale Microscale Thermophys. Eng.* **23**, 247 (2019).
- [22] J. Maassen and V. Askarpour, *APL Mater.* **7**, 013203 (2019).
- [23] N. D. Le, B. Davier, N. Izitounene, P. Dollfus, and J. Saint-Martin, *J. Comput. Electron.* **21**, 744 (2022).
- [24] Y. Hu, T. Feng, X. Gu, Z. Fan, X. Wang, M. Lundstrom, S. S. Shrestha, and H. Bao, *Phys. Rev. B* **101**, 155308 (2020).
- [25] K. Gordiz and A. Henry, *J. Appl. Phys.* **121**, 025102 (2017).
- [26] K. Esfarjani, G. Chen, and H. T. Stokes, *Phys. Rev. B* **84**, 085204 (2011).
- [27] S. Oktyabrsky and D. Y. Peide, *Fundamentals of III-V Semiconductor MOSFETs* (Springer, Berlin, 2010).
- [28] H. J. Joyce, Q. Gao, H. Hoe Tan, C. Jagadish, Y. Kim, J. Zou, L. M. Smith, H. E. Jackson, J. M. Yarrison-Rice, P. Parkinson *et al.*, *Prog. Quantum Electron.* **35**, 23 (2011).
- [29] J. A. del Alamo, *Nature (London)* **479**, 317 (2011).
- [30] L. S. Larkin, M. R. Redding, N. Q. Le, and P. M. Norris, *J. Heat Transfer* **139**, 031301 (2016).
- [31] J.-P. M. Péraud and N. G. Hadjiconstantinou, *Appl. Phys. Lett.* **101**, 153114 (2012).
- [32] See Supplemental Material at <http://link.aps.org/supplemental/10.1103/PhysRevMaterials.8.014604> for summarized results of DFT calculations.
- [33] G. Kresse and J. Hafner, *Phys Rev B* **47**, 558 (1993).
- [34] G. Kresse and J. Hafner, *Phys Rev B* **49**, 14251 (1994).
- [35] G. Kresse and J. Furthmüller, *Comput. Mater. Sci.* **6**, 15 (1996).
- [36] G. Kresse and J. Furthmüller, *Phys. Rev. B* **54**, 11169 (1996).
- [37] A. Togo and I. Tanaka, *Scr. Mater.* **108**, 1 (2015).
- [38] W. Li, J. Carrete, N. A. Katcho, and N. Mingo, *Comput. Phys. Commun.* **185**, 1747 (2014).
- [39] P. E. Blöchl, *Phys. Rev. B* **50**, 17953 (1994).
- [40] G. Kresse and D. Joubert, *Phys. Rev. B* **59**, 1758 (1999).
- [41] L. Lindsay, D. A. Broido, and T. L. Reinecke, *Phys. Rev. B* **87**, 165201 (2013).
- [42] Q. Hao, G. Chen, and M.-S. Jeng, *J. Appl. Phys.* **106**, 114321 (2009).
- [43] P. B. Allen and V. Perebeinos, *Phys. Rev. B* **98**, 085427 (2018).
- [44] J. M. Ziman, *Electrons and Phonons: The Theory of Transport Phenomena in Solids* (Oxford University Press, Oxford, 2001).
- [45] G. Chen, *Nanoscale Energy Transport and Conversion: A Parallel Treatment of Electrons, Molecules, Phonons, and Photons* (Oxford University Press, Oxford, 2005).
- [46] D. T. Morelli, J. P. Heremans, and G. A. Slack, *Phys. Rev. B* **66**, 195304 (2002).
- [47] O. L. Anderson, *J. Phys. Chem. Solids* **24**, 909 (1963).
- [48] V. Wang, N. Xu, J.-C. Liu, G. Tang, and W.-T. Geng, *Comput. Phys. Commun.* **267**, 108033 (2021).